Spinstand Control Characterization of an Electromagnetic Slider Microactuator

Mark D. Bedillion, Mahmut Karaman, and Patrick B. Chu, *Members, IEEE*

Abstract— **Increasing areal densities in disc drives require high performance servo tracking systems to attenuate runout. High bandwidth, large stroke microactuators are used to improve positioning accuracy by eliminating disturbances at higher frequencies. This paper details modeling and servo control of an electromagnetic slider microactuator designed at Seagate and its promise as a solution for high accuracy tracking control. The device has passive high frequency windage disturbance attenuation due to its structure. Controller design is developed for a single stage spinstand environment to show the device effectiveness.**

I. Introduction

HIGH performance disk drives demand track densities in the hundreds of thousands of tracks-per-inch (TPI) range [1,2]. High accuracy tracking is accomplished through passive disturbance reduction (air dampers) or through sophisticated, high bandwidth dual stage control systems. A disc drive servo system typically uses a voice-coil-motor (VCM) to position one or more recording heads relative to data tracks on magnetic discs. The recording heads are mounted on sliders, grooved micro-structures that allow the heads to fly passively over the media. The sliders are mounted on a flexible suspension, which in turn is mounted to the rigid structure to which the VCM is attached. In a dual stage system, a small, fast actuator is placed between the VCM and head to provide relatively high bandwidth, small stroke motion [3-11]. Dual stage designs have typically consisted of PZT actuated suspensions and MEMS or PZT actuated sliders.

The work described in this paper focuses on the use of a Seagate designed slider magnetic microactuator (MAGMA: MAGnetic MicroActuator) to improve tracking capability [6-8]. The MAGMA is an electromagnetic actuator that offers a large actuation stroke of 20μm, sufficient to cover several hundred tracks at 300kTPI and above while removing thermal drift. The MAGMA not only enables high bandwidth closed-loop servo for low frequency disturbance attenuation but also offers passive high frequency disturbance attenuation through its mechanical properties, as described in Section 3. Strain gauges provide relative displacement between the slider and suspension, which may be used to damp resonances during seeks or, in the tracking case, improve open loop performance during servo writing.

The implementation studied in this paper is on an Agilent spinstand. Controller design is only considered for a single stage; it is assumed that the VCM loop in a dual stage design will not be substantially affected by the choice of secondary stage controller. This assumption allows the device to be characterized at the head-gimbal assembly (HGA) level. Future work will consider the full dual stage control problem.

The paper proceeds as follows. Section 2 briefly details the MAGMA microactuator design features and properties. Section 3 models the MAGMA device. Section 4 provides a controller design using an inner/outer loop framework. Section 5 concludes.

II. The MAGMA Microactuator

The MAGMA device is an electromechanical micro-actuator with a slider attached so that the slider can have translational motion in the cross-track direction. Similar to a previous generation device reported earlier [6], MAGMA (Figure 1) has four key components including a magnet, the top and bottom keepers (for confining the actuator magnetic field), and a silicon body with a slider cavity suspended by four high-aspect ratio long beams (springs) and embedded metal coils. A patent for this basic design has been awarded to Seagate [7]. In addition, the device being reported here has strain gages integrated in the silicon body for position detection. MEMS design and fabrication will be detailed in a separate publication.

The MAGMA coil on the rotor is located directly under the magnet and top keeper. When a current is applied to the MAGMA coil, the induced magnetic field of the coil interacts with the magnet, thus generating a force which moves the rotor (and the slider inside the cavity of the rotor) laterally or cross-track. The magnetic force is counteracted by the spring force of the silicon beams.

Manuscript received March 1, 2005.

M.D. Bedillion is a Research Senior Engineer with Seagate Technology, Pittsburgh, PA 15222 USA (phone: 412-918-7243; fax: 412-918-7222; e-mail: mark.bedillion@ seagate.com).

M. Karaman is a Research Staff Member with Seagate Technology (e-mail: mahmut.karaman@seagate.com).

P.B. Chu is a Research Staff Member with Seagate Technology (e-mail: patrick.chu@seagate.com).

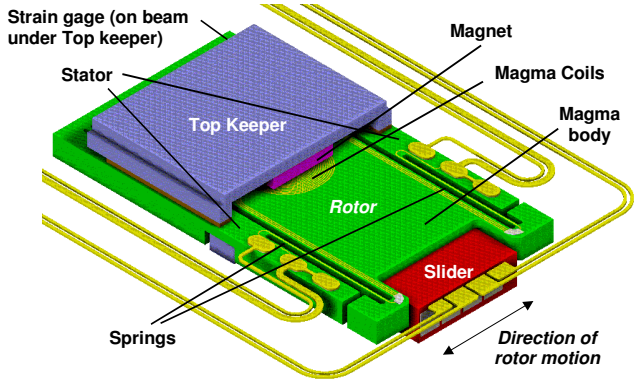

(a)

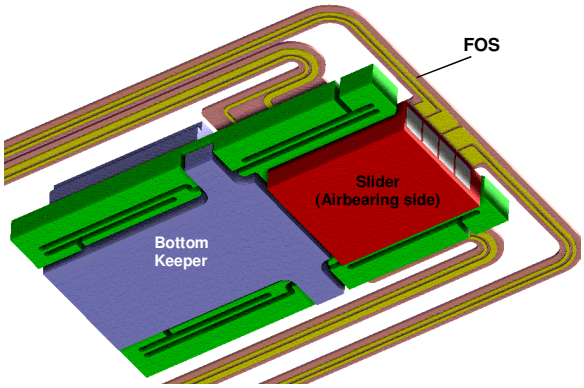

(b)

Fig. 1. (a) Top view and (b) bottom view of a MAGMA actuator CAD drawing with a slider attached to a FOS.

The MAGMA achieves a displacement of approximately ±10μm with maximum current applied. Its mechanical resonance is near 1.6kHz. This low resonance mode passively attenuates vibrations and disturbances applied to the suspension of frequencies higher than 1.6kHz. The large displacement and force output of MAGMA also enable high-bandwidth closed-loop servo of sliders as either a single-stage or a secondary-stage actuator.

Strain gages are embedded at the end of one of the springs (Fig. 1a). The piezo-resistive (PR) strain gages form a resistive half-bridge whose output reflects the relative displacement between the rotor and the stator. Closed-loop servo using the PR sensor can potentially improve the seeking performance in a disk drive. On the spin-stand where seek performance is not critical, closed-loop servo using the PR sensor may be used not only to improve servo tracking performance (Section IV) but also to attenuate the mass-spring mode during servo writing.

The tradeoffs of MAGMA's merits are its complexity and its large volume and mass. The size of the device is about 4.5 times larger than the slider, making it more susceptible to windage disturbances than a bare slider. The mass of the device (with a slider attached) is about 8 times heavier than a bare slider. The large mass unfortunately compromises suspension performance by lowering the resonance modes of a given suspension design. A short custom suspension has been designed with increased

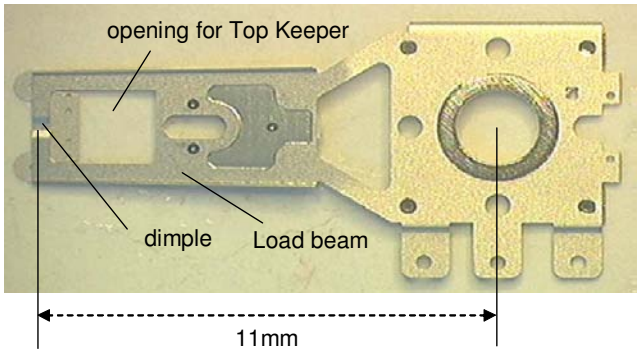

(a)

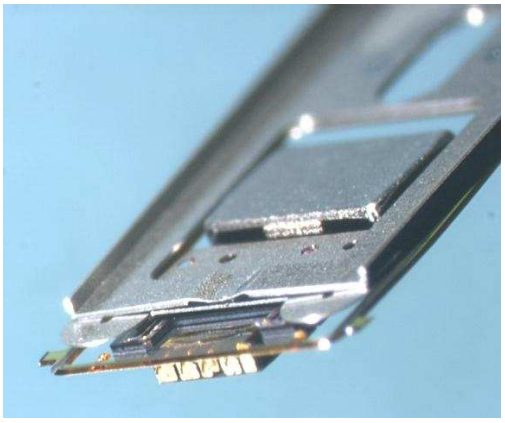

(b)

Fig. 2. Photos of (a) Custom suspension (Top view) and (b) MAGMA on custom suspension.

stiffness in its load beam for this reason (Fig. 2).

III. System Characterization

A. Mechanical Isolation

One of the most appealing features of the MAGMA microactuator is its high frequency disturbance isolation property. Assuming that the mass and stiffness of the suspension are such that the motion of the MAGMA does not produce significant suspension motion, the interaction between the suspension tip (MAGMA stator) and slider (MAGMA rotor) may be modeled as a one-way base excitation as shown in Fig. 3. With respect to a fixed reference point, the suspension tip (or MAGMA stator) cross-track motion due to windage and suspension base plate excitation is indicated by y(t) and the slider (or MAGMA rotor) motion denoted by x(t). For this simple mass-spring-damper system, the equation of motion of the slider can readily be identified as

$$M\ddot{x} + b(\dot{x} - \dot{y}) + k(x - y) = 0\,, \qquad (1)$$

where M is the total mass (MAGMA rotor and slider), b is the damping constant and k is the spring constant.

Moving terms involving suspension motion to the RHS and taking Laplace transforms leads to the following transfer

function relating recording head motion to suspension tip motion

$$\text{Transmission} = \frac{X(s)}{Y(s)} = \frac{2\zeta\omega_n s + \omega_n^2}{s^2 + 2\zeta\omega_n s + \omega_n^2}, \quad (2)$$

where ζ is the damping ratio and ω_n is the undamped natural frequency of the MAGMA rotor and slider.

Fig. 4 shows the Bode plots of Transmission and a second order system model of the MAGMA actuator transfer function (gain adjusted, with stator stationary) plotted together. The two transfer functions have similar responses at low frequency, but differ after the fundamental frequency. The difference is due to the damping between rotor and stator, which causes the actual isolation to be only 20dB/decade at high frequency.

B. Spinstand Characterization

Testing of the MAGMA HGA was performed on a spinstand. Experiments were carried out to characterize the dynamic performance of the MAGMA actuator and PR sensor. In these experiments, the suspension base plate is stationary and only the MAGMA actuator is actively driven. Measurement results of a selected HGA are presented as follows.

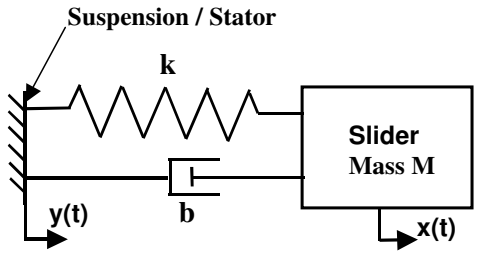

Fig. 3. MAGMA/Suspension Interaction. The dynamics are modeled as a one-way base excitation. A mass-spring-damper model effectively captures the MAGMA dynamics.

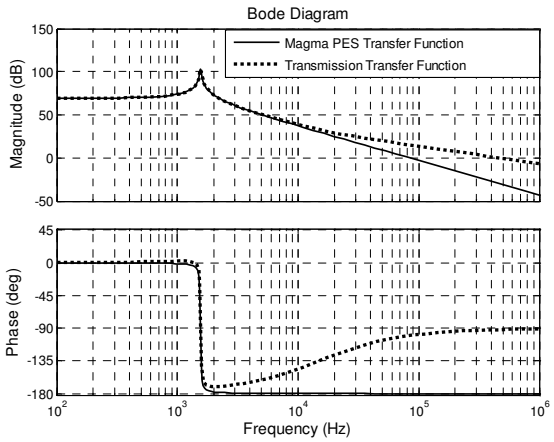

Fig. 4. Demonstration of Isolation. Suspension motion is not transmitted to the head above the mass-spring mode.

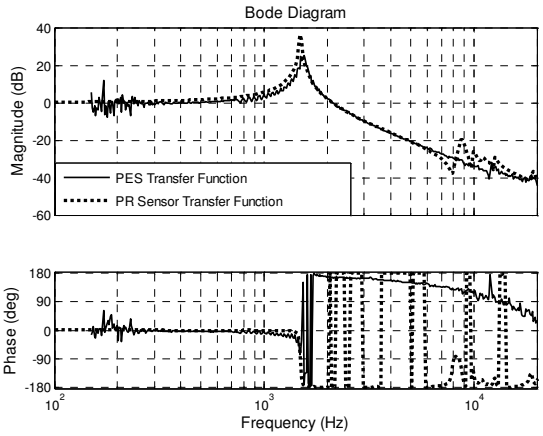

Fig. 5. Measured Transfer Functions. Note that the PR sensor transfer function contains suspension modes that are not present in the PES curve. Phase spikes in the PR sensor data are due to wrapping.

The MAGMA actuator response based on PES (solid curve) and PR sensor (dashed curve) measurements is plotted in Fig. 5. The MAGMA actuator PES response is characterized by a second order mass-spring system with natural frequency around 1500-1700 Hz, and damping ratio around 0.008-0.01.

The PR sensor response, however, displays additional (torsion) modes above 6-7 kHz. The difference between the PES and PR sensor measurements is due to the fact that the PR sensor measures the relative displacement between the rotor and stator of the MAGMA actuator (i.e., between the slider and the suspension tip) and picks up modes that are isolated by the dynamics of the MAGMA mass-spring system. In Fig. 5 the measurements are normalized.

The lightly damped fundamental mode is easily excited by windage disturbances, leading to large PES errors at its frequency during open-loop operation. This large error eliminates the possibility of notch filtering the mass-spring mode; either phase stabilization or a high-bandwidth design is required. High-bandwidth design in the PES loop is facilitated by a very smooth high frequency roll-off. High-bandwidth design in the PR sensor loop is made difficult by the multiple torsion modes shown in Fig. 5. An additional feature not visible in Fig. 5 is the MAGMA actuator's low stiffness relative to conventional suspensions. This low stiffness degrades the device's low frequency disturbance rejection in open-loop, which places a large low frequency gain requirement on the control loops.

IV. CONTROLLER DESIGN

This section considers two strategies for tracking controller design using MAGMA as a single-stage positioner: one using only PES feedback, and one using both PES and PR sensor feedback. The suspension base plate is assumed to be stationary, although the HGA is exposed to windage and

other system vibrations. Tracking controller design for the PES loop is made difficult by the inherent 180° phase shift of the mass-spring mode coupled with system delay. In this paper a 25μs total delay is assumed from 50kHz sampling and computation in the PES loop, and a 200kHz sampling rate and 2.5μs computation delay are used in the PR sensor loop. The large PES loop computation delay accounts for the time needed to read multiple PES bursts and transfer delays between the demodulator and the controller. The necessity of adding phase lead around the crossover frequency limits the ability of the controller to attenuate low frequency disturbances. An inner-outer loop design is advantageous because the inner loop can be closed at a higher sampling rate, thereby attenuating the large input disturbance at the mass-spring mode and mitigating the effects of sampling delay.

A. *Dual Loop Design*

The loop block diagram for the dual-input, single-output controller design is given in Fig. 6, where G_{pr} is the transfer function from the input to the PR sensor output and G_m is the transfer function from the input to PES output. Block diagram algebra yields

$$y = \frac{1 + C_{pr}G_{pr}}{1 + G_m C_m C_{pr} + C_{pr}G_{pr}} d_o + \frac{G_m}{1 + G_m C_m C_{pr} + C_{pr}G_{pr}} d_i + \frac{G_m C_m C_{pr}}{1 + G_m C_m C_{pr} + C_{pr}G_{pr}} r \quad . \tag{3}$$

Closing the inner PR sensor loop at a frequency higher than the mass spring mode effectively changes the frequency range of passive attenuation (as discussed in Section III). Low frequency disturbances come from thermal drift of the tracks relative to the recording head, spindle wobble, and broadband windage excitation. The latter is particularly relevant to the MAGMA device due to its low stiffness relative to conventional suspensions. In this paper, the assumption is that low frequency disturbances are dominant, and the approach will be to maximize the bandwidth of the inner loop to reduce the effects of sampling delay and at the same time make the system immune to low frequency input disturbances.

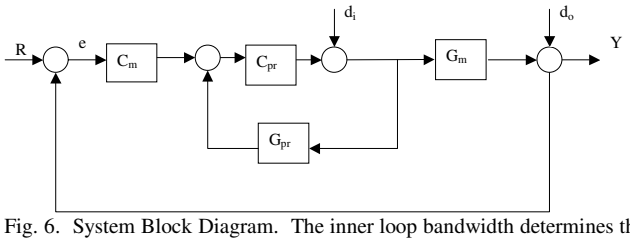

Fig. 6. System Block Diagram. The inner loop bandwidth determines the range of passive input disturbance isolation, while the outer loop attenuates output disturbances.

The design models based on data from Fig. 5 are shown in Fig. 7 and the μ synthesis block diagram is shown in Fig. 8. The PES response is modeled as a second order system with delay, and the PR sensor model is similar but with an additional torsion mode. W_{dist} and W_{perf} combine to place a weight on the output sensitivity function, W_m places a weight on the additive uncertainty, and W_{act} places a weight on the control signal. The chosen weights are shown in Fig. 9 and the plant with uncertainty envelope is shown in Fig. 10. The disturbance weight in Fig. 9 is used to account for windage excitation of the lightly damped MAGMA resonance mode. The performance weight provides low frequency disturbance rejection and defines the system bandwidth.

Fig. 11 shows the achieved sensitivity function. The controller is not able to achieve the desired sensitivity function, most likely due to the large torsion mode in the PR sensor design model of Fig. 7 and its associated uncertainty. The torsion mode limits the bandwidth with which the inner loop may be closed and therefore limits any potential phase gain from the PR sensor's high sampling rate.

The outer loop must be designed to attenuate low frequency suspension motion (below the mass-spring mode) and output disturbances, which the inner loop cannot compensate. The system that the outer loop must control is

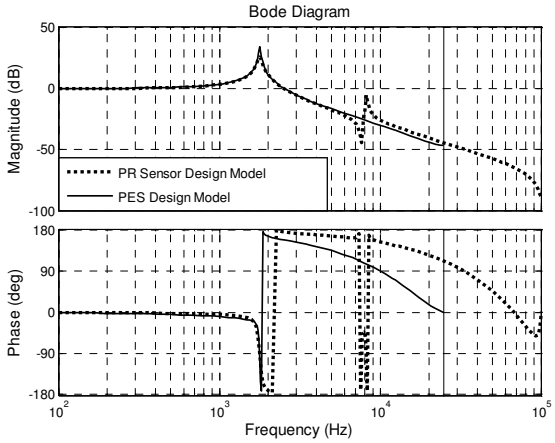

Fig. 7. Design Models. The effects of sampling rate on the MAGMA transfer function are not as severe in the PR sensor response. The gains have been normalized.

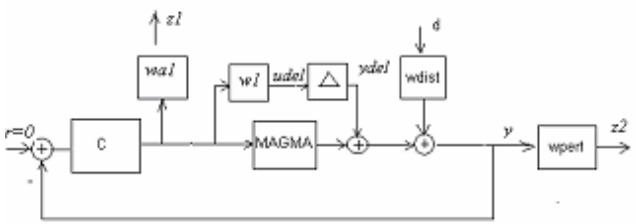

Fig. 8. μ Synthesis Block Diagram. The design uses additive uncertainty and disturbance, performance, and actuator weights.

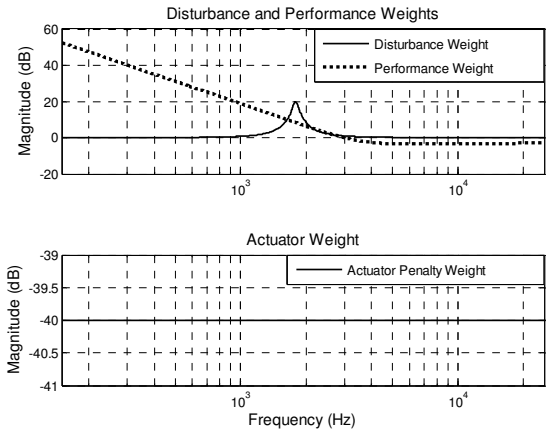

Fig. 9. Weighting Functions. The disturbance and performance weights attenuate disturbances at the MAGMA mass-spring mode and at low frequencies.

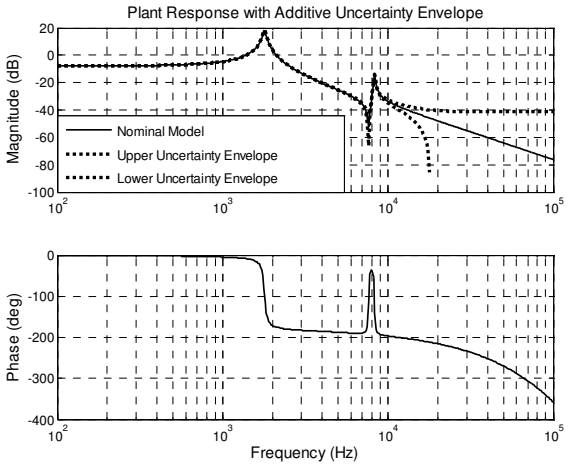

Fig. 10. Response with Uncertainty Envelope. The model is relatively certain until after the torsion mode.

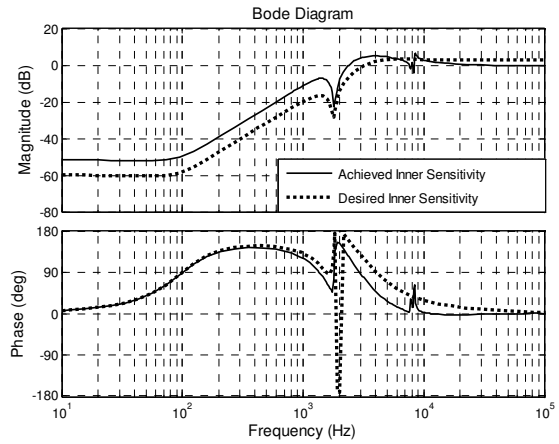

Fig. 11. Inner Loop Sensitivity Function. The inner loop design does not meet the design specifications, mainly due to the torsion mode near the crossover frequency.

shown in Fig. 12 and is given by

$$G_{outer} = \frac{C_{pr} G_m}{1 + C_{pr} G_{pr}} \quad . \tag{4}$$

This function essentially behaves like the complementary sensitivity function of the inner loop because the PES and PR sensor transfer functions are similar. The key feature from the design perspective is that the phase is maintained above 180° until approximately 6kHz. This is an advantage over designing for the PES transfer function (also shown in Fig. 12).

The outer loop design uses design weights shown in Fig. 13 and similar additive uncertainty to the inner loop, resulting in the performance shown in Fig. 14. In this case the design is able to closely match the desired sensitivity function.

B. PES Loop Controller Design

The PES loop controller design uses the same controller and uncertainty weights as the inner loop design because the

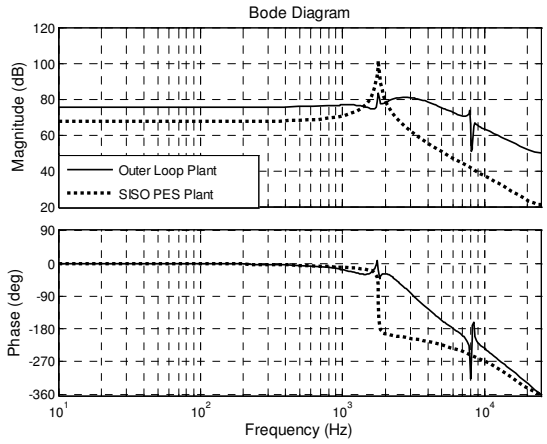

Fig. 12. Outer Loop Plant and MAGMA PES Transfer Function. Note the improved phase response of the outer loop plant.

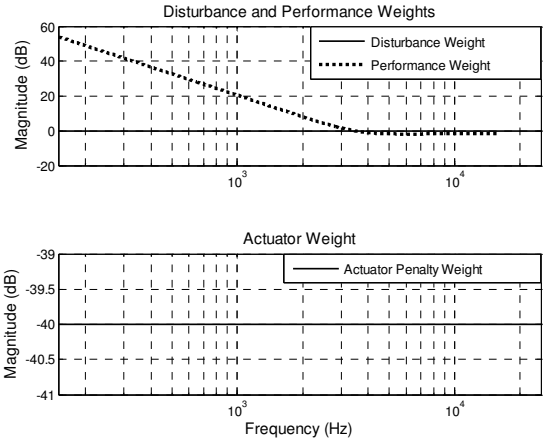

Fig. 13: Outer Loop Design Weights. The outer loop does not need to account for input disturbances at the MAGMA mass-spring frequency.

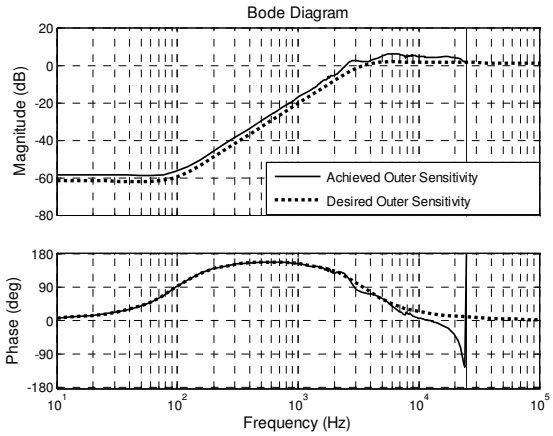

Fig. 14. Outer Loop Sensitivity Function. The outer loop design comes close to meeting the design requirements.

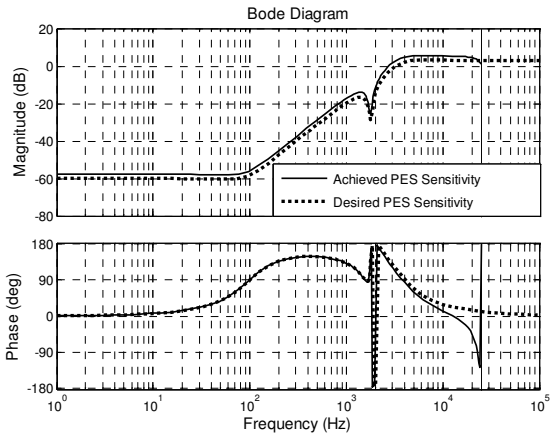

Fig. 15. PES Loop Sensitivity Function. The PES sensitivity function comes very close to meeting the specified design.

plants are very similar. Designed and achieved functions are shown in Fig. 15. Note that the PES loop comes closer to achieving the desired function than the inner loop despite its lower sampling rate.

To compare performance between the two designs, input and output sensitivity functions are compared. For the dual loop design the transfer functions are given in (3). Figs. 16 and 17 show that the dual loop design has similar attenuation for output disturbances but clearly superior performance for input disturbances. The dual loop design was not able to mitigate sampling rate effects because of the large torsion mode in the PR sensor design model. However, the improved input sensitivity function gives the MAGMA low frequency performance competitive with non-microactuated suspensions despite its low mass-spring mode. Note that although the dual loop output sensitivity function does not show attenuation at the mass-spring mode, it has the same input sensitivity performance as the PES loop at the mass-spring frequency.

V. CONCLUSIONS

This paper has summarized a slider-level linear electromagnetic microactuator and its use in tracking control. The Seagate MAGMA design has the advantage that it passively attenuates high frequency disturbances that act on the suspension. The controller design uses both PES feedback and feedback from a piezo-resistive sensor that measures the motion of the slider relative to the suspension. The inner loop is intended to minimize the effects of sampling delay and low frequency input disturbances, while the outer loop is designed to maximize disturbance rejection. The sampling rate mitigation property is lost due to the PR sensor torsion mode, but the dual loop design does provide strong input disturbance rejection at low frequencies. This input disturbance rejection allows the MAGMA to achieve performance comparable to a standard suspension at low frequencies.

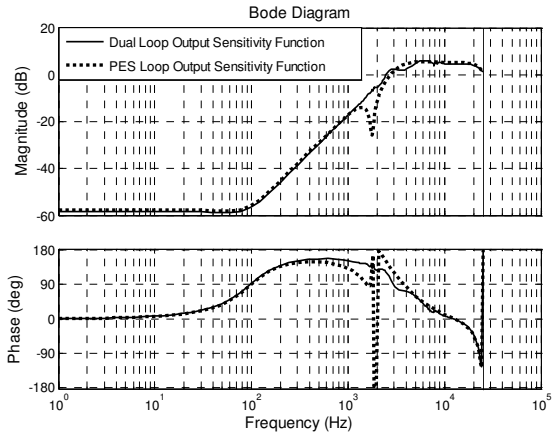

Fig. 16. Dual Loop vs. SISO Control Ouput Sensitivity Functions. The dual loop design achieves similar low frequency attenuation. Closing the inner loop removes the disturbance at the mass-spring mode.

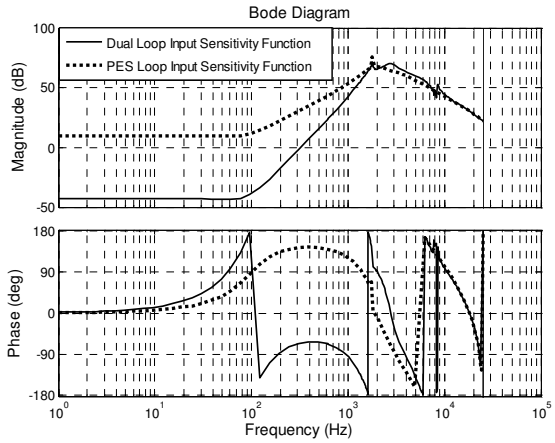

Fig. 17. Dual Loop vs. SISO Control Input Sensitivity Functions. The dual loop design has significantly superior performance.

ACKNOWLEDGMENT

The authors of this report would like to acknowledge the support of Seagate's Advanced Mechanical Technology team (led by Zine Boutaghou) which developed the MEMS device. Special thanks to Roger Hipwell and Kou Vang (for MEMS fabrication), Jennifer Engebrit and John Hurley (for device and HGA assembly), Andy White and John Morris (for sensor electronics and servo input).

REFERENCES

[1] Tarnopolosky, Giora J., "Hard Disk Drive Capacity at High Magnetic Areal Density", in *IEEE Transactions on Magnetics*, Vol. 40, No. 1, January 2004, pp. 301-306.

[2] Wood, R.W., Miles, J. and Olson, T., "Recording Technologies for Terabit per Square Inch Systems," in *IEEE Transactions on Magnetics*, Vol. 38, No. 4, July 2002, pp. 1711-1718.

[3] Evans, R.B. and Karaman, M., "Closed-loop Testing of a Suspension Based Piezoelectric Microactuator," in *Digest of the Asia-Pacific Magnetic Recording Conference* , pp. WA2/1-WA2/2

[4] Koganezawa, S., Uematsu, Y., Yamada, T., Nakano, H., Inoue, J. and Suzuki, T., "Dual-Stage Actuator System for Magnetic Disk Drives Using a Shear Mode Piezoelectric Microactuator," in *IEEE Transactions on Magnetics*, Vol. 35, No. 2, pp. 988-992.

[5] Hirano, T., Fan, L.S., Lee, W.Y., Hong, J., Imaino, W., Pattanaik, S., Chan, S., Webb, P.R., Horowitz, R., Aggarwal, S. and Horsley, D., "High-Bandwidth High-Accuracy Rotary Microactuators for Magnetic Hard Disk Drive Tracking Servos", in *IEEE/ASME Transactions on Mechatronics,* Vol. 3, No. 3, September 1998, pp. 156-165.

[6] Hipwell, R., Bartholomew, K., Bonin, W., Boutaghou, Z. and Lateef, A., "MEMS Enhance Hard Disk Drive Performance," in *Unaxis Chip,* No. 8, pp. 28-33.

[7] Crane, P., Bonin, W., Hipwell, R., and Boutaghou, Z., "Moving coil micro actuator with reduced rotor mass," U.S. Patent 6,614,628, September 2, 2003.

[8] Hipwell, R., Walter, L., Bonin, W., Wissman, B., and Boutaghou, Z., "Structure and fabrication process for integrated moving-coil magnetic micro-actuator," U.S. Patent 6,661,617, December 9, 2003.

[9] Okada, K., Lou, Y., Gao, P., Qin, B., Ong, E. H. and Guo, G., "A Novel In-slider Piezoelectric Microactuator for Hard Disc Drives," in *Digest of the Asia-Pacific Magnetic Recording Conference*, 2002, pp. 27-29.

[10] Imamura, T., Katayama, M., Ikegawa, Y., Ohwe, T., Koishi, R. and Koshikawa, T., "MEMS-Based Integrated Head/Actuator/Slider for Hard Disk Drives," in *IEEE/ASME Transactions on Mechatronics*, Vol. 3, No. 3, pp. 166-174.

[11] Shroeck, S.J. and Messner, W.C., "On Controller Design for Linear Time-Invariant Dual-Input Single-Output Systems," in *Proceedings of the American Control Conference*, 1999, Vol. 6, pp. 4122-4126